Collective Deceleration of Laser-Driven Electron Bunches

S. Chou (周紹暐),[1,2,*] J. Xu (徐建彩),[1,3] K. Khrennikov,[2] D. E. Cardenas,[1,2] J. Wenz,[2] M. Heigoldt,[2] L. Hofmann,[1,2] L. Veisz,[1,4] and S. Karsch[1,2]

[1]*Max-Planck Institut für Quantenoptik, 85748 Garching, Germany*

[2]*Department für Physik, Ludwig-Maximilians Universität, 85748 Garching, Germany*

[3]*State Key Laboratory of High Field Laser Physics, Shanghai Institute of Optics and Fine Mechanics, Chinese Academy of Sciences, P. O. Box 800-211, Shanghai 201800, China*

[4]*Department of Physics, Umeå University, SE-901 87 Umeå, Sweden*

(Received 1 March 2015; revised manuscript received 19 August 2016; published 27 September 2016)

Few-fs electron bunches from laser wakefield acceleration (LWFA) can efficiently drive plasma wakefields (PWFs), as shown by their propagation through underdense plasma in two experiments. A strong and density-insensitive deceleration of the bunches has been observed in 2 mm of 10^{18} cm^{-3} density plasma with 5.1 GV/m average gradient, which is attributed to a self-driven PWF. This observation implies that the physics of PWFs, usually relying on large-scale rf accelerators as drivers, can be studied by tabletop LWFA electron sources.

DOI: 10.1103/PhysRevLett.117.144801

Laser and plasma wakefield accelerators (LWFA and PWFA) are promising concepts to boost the acceleration gradient from $\approx$ 100 MV/m in conventional rf accelerators up to 10's to 100's GV/m [1]. Laser-driven (i.e., LWFA-type) relativistic electron sources are routine and have been demonstrated by many laboratories, e.g., Refs. [2–9], delivering $\lesssim 5$ fs FWHM and multi-kA bunches [10–12]. However, the electron energy from single-stage LWFA is mainly limited by dephasing, since the highly relativistic accelerated electrons eventually outrun the wakefield whose phase velocity is subluminal ($v_{\mathrm{ph}} < c$) [13]. In contrast, PWFA driven by high-energy charged particle beams is already moving at $v \approx c$, and so suffers much less from dephasing. Also, particle beams can stay focused over much longer distances than optical laser beams. However, PWFA requires high energy and current-density bunches in order to drive high-gradient ultrarelativistic wakefields [14,15]. These bunches are only provided by a few large-scale facilities, such as, e.g., SLAC, CERN, and DESY, where beam time for accelerator research and development is usually limited [16–20]. LWFA bunches, widely available in university-scale laboratories around the world, already possess most of the required parameters for driving PWFAs: High charge density, ultrahigh current, and controllable single or multiple bunch structure. Except for final energy and average power, they are ideal for studying beam-driven wakefield physics in a small-scale model, thus complementing large facilities for detailed parameter studies. Even the typical spectral bandwidth of LWFA beams is of low concern for that kind of application. Concerning laser-driven acceleration, hybrid PWFA driven by LWFA beams has also been proposed to double the achievable electron energy for a given laser energy [21]. Therefore, realizing a beam-driven wakefield with LWFA accelerated beams would be a major step forward for studying future high-gradient accelerators.

In this Letter, we present the first experimental evidence of collective deceleration of LWFA electron beams inside mm-scale plasma in two independent experiments, which can only be explained by the generation of a strong beam-driven wake. The first experimental setup is illustrated in Fig. 1. The ATLAS 60 TW Ti:sapphire laser system was used to drive the primary electron bunches. The laser pulses of 870 mJ were focused by a parabolic mirror with $f/13$

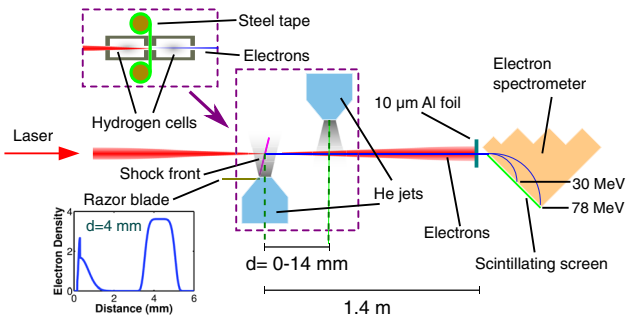

FIG. 1. Experimental setup. Jet 1 (left), which had a 300 μm exit aperture and 1000 μm FWHM density profile along the laser propagation axis, was used to generate stable and tunable monoenergetic electron bunches by shock-front injection. The shock was generated by inserting a razor blade into the supersonic flow. Jet 2 had 1500 μm exit aperture and 1500 μm flattop density profile, and its center was placed between $d = 0$ and 14 mm behind the shock. Bottom left: electron density profile based on interferometry and Rayleigh scattering. The density is normalized to 10^{18} cm^{-3}. The density of jet 1 without the shock front was fixed at 1.7×10^{18} cm^{-3} while the density of jet 2 was changed between $(1.2–4.8) \times 10^{18}$ cm^{-3}. Top left: setup of the double gas cells.

optical geometry to a 15.9 μm FWHM spot and delivered 550 mJ within the first Airy ring with 28 fs duration on target. The peak intensity was 6.2×10^{18} W/cm^2, and the energy stability is better than 5%. A permanent magnet spectrometer with an absolutely charge-calibrated scintillating screen was used as an electron detector [22], which can resolve electron energies from 2 to 78 MeV with few percent resolution [23], and has an angular aperture of 29.4 mrad. The targets were two supersonic helium jets with adjustable separation and separately controlled densities. The density fluctuation was $< 0.8\%$. In jet 1, shock-front injection resulted in tunable and stable electron spectra (injection probability $> 95\%$, rms peak energy fluctuation < 2 MeV at 36 MeV peak energy, standard error of charge stability $\approx 1\%$) as observed in Ref. [2]. Typical spectra are shown in Fig. 2(a). These bunches first propagated through a vacuum gap, before interacting with jet 2. The gas profile of both jets plus the shock front were characterized off-line by interferometry and Rayleigh scattering [24]. These measurements confirmed that there is no detectable interference between the two jets when $d > 2$ mm, where d is the distance between the shock front in jet 1 and the middle of jet 2.

A consistent deceleration of the majority of electrons was observed with jet 2. Figures 2(c)–2(d) show two sets of spectra for different separations; since the shock-front injection provides a highly stable LWFA electron source [Fig. 2(b)], the observed broadening of the spectra after jet 2 was clearly not the shot-to-shot fluctuation of the injected bunches. Although the spectra were found to be unstable especially compared to the case without jet 2, a similar pattern in the spectra was visible. Figure 3(a) shows the average spectra after jet 2 as a function of separation. As d decreased, the spectra became broader and skewed towards the low energy side. In the closest cases, an additional low-energy peak around 15 MeV was generated, possibly due to re-acceleration as indicated by the simulations. Since the decelerated spectra were not monoenergetic, we define the remaining energy fraction (REF) to characterize the total bunch energy after interaction, $\mathrm{REF} \equiv \int ES(E)dE / \int ES_0(E)dE$, where $S(E)$ is the electron spectrum after jet 2, and $S_0(E)$ is the spectrum after jet 1. Likewise, the remaining charge fraction (RCF) characterizes the charge loss: $\mathrm{RCF} \equiv \int S(E)dE / \int S_0(E)dE$.

The REFs and RCFs after jet 2 were found to be identical to within 20% even for a fourfold change in jet 2's density and seemed to depend mainly on d as depicted in Figs. 4(a) and 4(b), respectively. The results affected by gas turbulence ($d < 2$ mm) were left out of the analysis. REF and RCF decreased monotonically with the distance between the two jets. The highest loss of over 94% was observed at $d = 3.5$ mm before gas interference took effect. At this distance, the peak number density of the electron beam is slightly above 1.2×10^{18} cm^{-3}, exceeding the lowest background electron density in jet 2. As it will be shown later, the self-focusing of the electron beam increases the peak density far above that of the background density even for the densest case (4.8×10^{18} cm^{-3}) in the experiment. The estimated average stopping power from the first momentum of the spectrum corresponds to a 5.1 GV/m deceleration gradient, and the peak stopping power can be estimated by the secondary peak around 15 MeV, which shows a gradient > 14 GV/m. These values exceed regular collisional and radiative energy loss [25] as well as betatron radiation loss [26] by a factor of $> 10^4$. The only possible

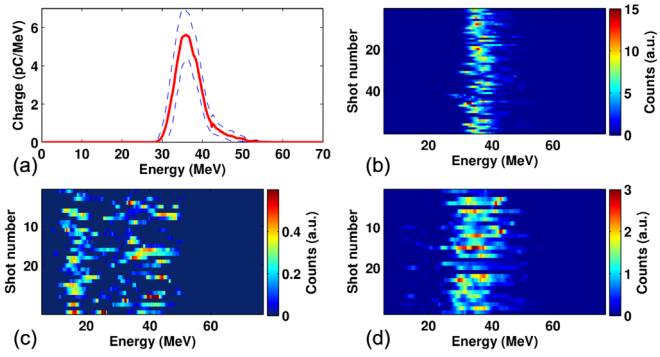

FIG. 2. Electron spectra. (a) Average spectrum (solid line) and root-mean-square (dashed line) from over 60 consecutive shots. The shock-front configuration was used to generate 35.8 ± 0.3 MeV, 44.3 ± 1.5 pC electrons with an average FWHM divergence 6.9 ± 0.17 mrad. (b) Consecutive shots of stable shock-front injected bunches without jet 2. (c) Decelerated spectra with $d = 3.5$ and 3.6×10^{18} cm^{-3} electron density in jet 2. (d) Decelerated spectra with $d = 6.5$.

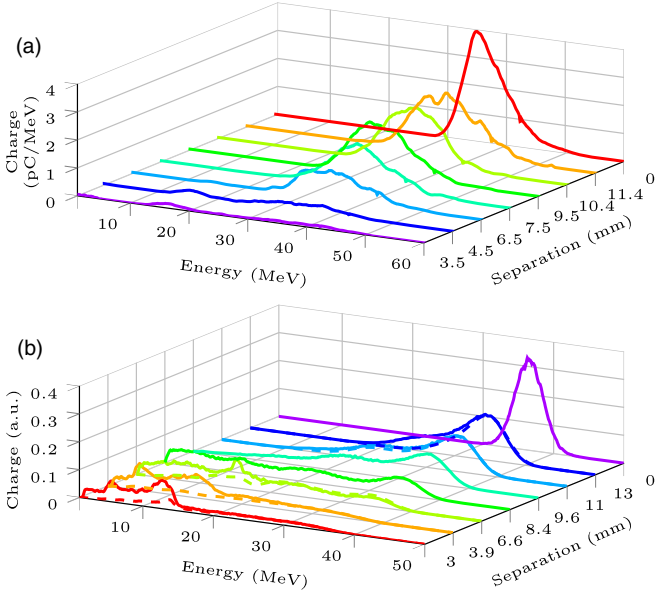

FIG. 3. Summary of spectra as a function of separation between two jets. (a) Average spectra from the experimental results. (b) Results from simulations where the solid lines show total spectra, and dashed lines below them are the spectra of electrons with divergence below 30 mrad.

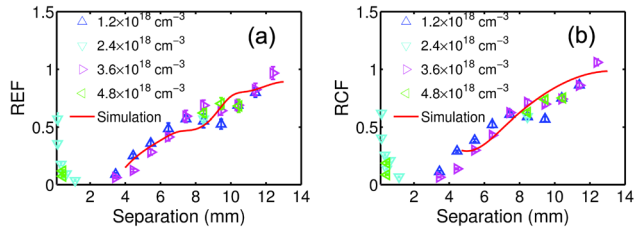

FIG. 4. Properties of electron bunches after interaction with jet 2. (a) REF from measurement and simulation vs separation. (b) Comparison of total RCF from experiment and 30 mrad full-divergence-limited RCF from simulations.

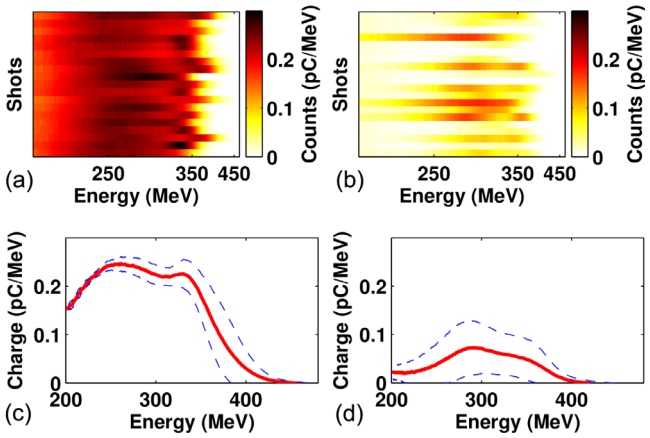

FIG. 5. Results of the second experiment utilizing double hydrogen-filled gas cells separated with a steel tape. The pressure in both cells was 140 mbar, corresponding to 6.8×10^{18} cm^{-3} assuming complete ionization. (a) Spectra from double gas cell, cell 2 evacuated. Total charge 37.80 ± 0.89 pC. (b) Spectra when both cells are filled. The average charge 8.42 ± 1.50 pC. (c) and (d) The average spectrum of (a) and (b), respectively. The average *observed* REF $= 0.23 \pm 0.041$ and RCF $= 0.22 \pm 0.040$.

explanation is collective stopping of the electrons by plasma (i.e., wake-) fields in jet 2 [27–29]. According to the simulations below, the charge loss is a direct consequence of the collective energy loss, since decelerated electrons scatter out of the wake.

There is solid circumstantial evidence that rules out a substantial deceleration by a wakefield driven in jet 2 by the residual laser: Since the electron energy in jet 1 was far below the 3D nonlinear dephasing limit ([30]) of 472 MeV, the bunch is located ≈ 25 μm behind the laser. Free-space propagation between the jets does not change this distance noticeably (< 1 μm/cm). If a laser-driven wakefield would dominate the observed deceleration, a fourfold change in density of jet 2 and hence a twofold change in plasma wavelength would place the electron bunch into a varying phase relative to such a possible laser-driven wakefield. This would lead to varying acceleration or deceleration, which was not observed as shown in Fig. 4, ruling out any strong influence of the residual laser wakefield.

In order to completely exclude any influence of the laser, an additional experiment using two hydrogen-filled 7 mm long gas cells was performed. They were separated by a 10 μm steel tape which was advanced after each shot, completely blocking the laser after cell 1. The 26 fs, 1.7 J laser pulse was focused by an $f/19$ parabolic mirror to a 22 μm FWHM spot on the target. Cell 1 was operated in the self-injection LWFA regime. Any plasma in cell 2 is generated by field ionization in the Coulomb field of the LWFA bunch [31] due to the small source size and low divergence after cell 1 [32,33], and the ratio between the peak density of the LWFA bunch and the background plasma is $\gg 1$. The results are shown in Fig. 5. Electrons were detected above the 200 MeV cutoff of the electron spectrometer resulting in a $> 70\%$ total energy and charge loss with gas in cell 2, while the original high energy front around 400 MeV was preserved. This observation is consistent with the double-jet experiment and proves that major deceleration is indeed caused by beam-driven wakefields.

In order to draw more conclusions from the double-jet experiment, we used 3D particle-in-cell simulations with OSIRIS [34] to model the wakefield from either the laser or e-beam driver. In the following, we first rule out strong laser-driven wakefields before comparing purely beam-driven wakefields to the experiment in a 2nd set of simulations.

In order to compare a maximum amplitude ratio of laser- and beam-driven wakefields, the laser was modeled as a Gaussian pulse with the same parameters as in the experiment and the electron bunch by a bi-Gaussian distribution $n_b e^{-(\xi^2/2\sigma_z^2)} e^{-(r^2/2\sigma_r^2)}$, where n_b is the peak density, σ_r is the bunch size, which is estimated by the measured divergence, and σ_z is the bunch length. The density profile used in simulations is shown in the inset of Fig. 1. A simulation of both laser and electron bunches requires a large volume while fully resolving the laser oscillations and is computationally very expensive. Therefore, only the shortest jet separation ($d = 3$ mm) was modeled as a worst-case scenario. The simulation yields $(E_{e-\max}/E_0) = 0.27$ and $(E_{l-\max}/E_0) = 0.06$ at the entrance of jet 2, where $E_{e-\max}$ and $E_{l-\max}$ are longitudinal magnitudes of the electron- and laser-driven wakefield, respectively, and E_0 is the cold nonrelativistic wave breaking field [13]. These values are similar to the analytical formula of the linear wakefield which gave $(E_{e-\max}/E_0) = 0.31$ and $(E_{l-\max}/E_0) = 0.1$ [35,36]. The analytical calculation also shows that $E_{e-\max}/E_{l-\max}$ increases for larger jet separation. As will be shown below in contrast to the laser wakefield, the plasma wakefield increases significantly after propagating in the 2nd plasma due to self-focusing of the electron bunch. Therefore, $E_{e-\max}/E_{l-\max}$ further increases up to 30. From these results we conclude that in a second set of simulations it is sufficient to assume only an electron drive bunch for describing the wakefield in jet 2. This conclusion is supported by the results of the second experiment where only a PWF decelerates the electrons.

In the second set of simulations, the default parameters were $\sigma_z = 1.4$ fs, $n_p = 3.6 \times 10^{18}$ cm^{-3}, and σ_r was variable $n_b/n_p = 11.5/{\sigma_r}^2(\mu\text{m})$. Varying the energy spread, plasma density up-ramp and the density profile shape had negligible influence on the final REF. Also the REF was found to only weakly depend on n_p and σ_z. Because of the very short pulses ($k_p\sigma_z = 0.13$–0.26, $\sigma_r/\sigma_z > 1$) far from the matching condition, i.e., $k_p\sigma_z \approx \sqrt{2}$ and $\sigma_r/\sigma_z \ll 1$; the well-known ${\sigma_z}^{-2}$ scaling law for $E_{e-\max}$ [37] is not applicable for our parameters.

Finally, we compare the experimentally determined REF with the simulation result for different initial beam sizes. This yields the bunch size as a function of separation, as shown in Fig. 4(a). The best fit requires 2 times lower divergence than what was measured. Figures 6(a)–6(f) illustrate one example of a typical bunch evolution from the simulation, where the spatial scale depends on the initial bunch diameter. Two distinguishable phases are visible after the bunches enter a plasma [I–II in Fig. 6(a)]. In phase I, the front side of the bunch expels the plasma electrons and drives a weak wakefield [Fig. 6(c)]. The back side of the bunch then experiences a strong focusing due to the static electric field of ions and self-driven magnetic field [39]. The focusing increases the peak density by almost 4 times [Fig. 6(d)], thus enhancing the wakefield which quickly decelerates the electrons in the tail of the bunch and causes a fast drop in the REF curve in Fig. 6(a). During deceleration, the electron energy spectrum gets broader because the head and tail of the electron bunch both sit the nonuniform longitudinal field regions as shown in Fig. 6(b). The process continues until phase II where the majority of the electrons are decelerated below the phase velocity of the plasma wave and get retrapped into the accelerating phase of the wave [Fig. 6(e)]. When the rate of energy loss from the driving part is comparable to the rate of energy gain of the trapped part, the decrease in REF reaches saturation and forms a shoulder. This coincides with the longitudinal position where the density in the second electron bunch exceeds that of the first, generating a second peak in the peak density curve [green line in Fig. 6(a)]. Later, the peak density and the total charge of the first bunch decreases beyond the point at which the wakefield is maintained [Fig. 6(f)]. In this specific case, corresponding to an intermediate separation of the jets, the REF amounted to ≈0.5. For smaller separations, also in the simulations the REF reaches values of ≈0.

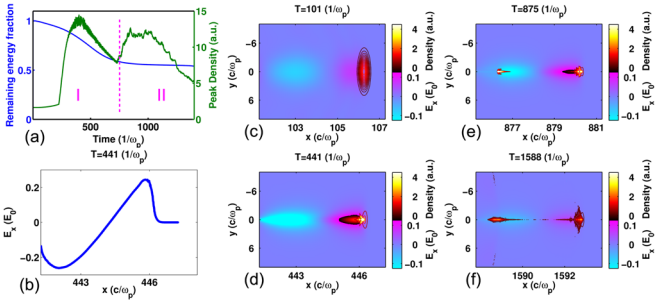

FIG. 6. Example of the simulated electron bunch evolution. The original bunch parameters are $\sigma_r = 6.1$ μm (corresponding to $d \approx 6$ mm), $\sigma_z = 1.4$ fs, $n_p = 3.6 \times 10^{18}$ cm^{-3}, and $n_b/n_p = 0.31$. The density profile was a step function, starting at $t = 47$. (a) Peak electron bunch density and REF vs time. After reaching quasistatic saturation [38] at $t \sim 700$, the value of the peak density jumps between the main driver and secondary bunch ($\sim 4c/\omega_p$ behind main driver). (b) The magnitude profile of the longitudinal wakefield. (c)–(f) Bunch density and longitudinal electric field at different time steps.

In conclusion, the trend of REF in Fig. 4(a) can be explained as follows: More electrons lose more energy for smaller jet separation, because the wakefields are enhanced by the stronger self-focusing of smaller bunches. In the case of very small separation, some of the decelerated electrons got considerably re-accelerated and generate secondary peaks around 15 MeV in spectra, which were visible in both experiment [Fig. 3(a)] and simulation [Fig. 3(b)]. Note that we only observe electrons within the spectrometer's solid angle. The simulation shows that due to the larger emission angle of low-energy electrons this leads to a suppression of the low energy part of the measured electron spectrum [Fig. 3(b)] and an apparent charge loss [Fig. 4(b)]. The effect is small, however, since the fraction of electrons outside this solid angle contributed to less than 20% of the final beam energy. Therefore, the dominant energy loss process was the deceleration in the wake.

In conclusion, we have observed strong energy loss of LWFA electrons in a plasma, which is attributed to a self-driven collective wake excitation. The results have been validated in a separate experiment and compared with simulations. The decrease in stopping power for larger distances to the stopping target is mainly caused by beam expansion. The large peak deceleration gradient, > 14 GV/m, shows the possibility to minimize the size of a beam dump dramatically [38]. Moreover, since LWFA electron bunches are much denser than conventional bunches, they can drive wakefields in much higher density plasmas compared to existent PWFA experiments [18–20]. This property is useful not only for building a tabletop PWFA test bench, but also to boost electron energy as an afterburner after dephasing or laser depletion in LWFA [13,21].

We would like to thank Ferenc Krausz for support of the project. The work is supported by the Cluster of Excellence MAP (EXC158), DFG Project Transregio TR18, the Euratom research and training programme 2014-2018 under Grant Agreement No. 633053 within the framework of the EUROfusion Consortium, and the Max- Planck-Society. We also acknowledge FCT (Portugal) and the IST Lisbon for the access to OSIRIS.

*swchou@mpq.mpg.de

[1] A. W. Chao and M. Tigner, *Handbook of Accelerator Physics and Engineering*, 2nd ed. (World Scientific, Singapore, 2013).

[2] A. Buck, J. Wenz, J. Xu, K. Khrennikov, K. Schmid, M. Heigoldt, J. M. Mikhailova, M. Geissler, B. Shen, F. Krausz, S. Karsch, and L. Veisz, Phys. Rev. Lett. **110**, 185006 (2013).

[3] W. P. Leemans, B. Nagler, A. J. Gonsalves, C. Tóth, K. Nakamura, C. G. R. Geddes, E. Esarey, C. B. Schroeder, and S. M. Hooker, Nat. Phys. **2**, 696 (2006).

[4] X. Wang *et al.*, Nat. Commun. **4**, 1988 (2013).

[5] K. Schmid, A. Buck, C. M. S. Sears, J. M. Mikhailova, R. Tautz, D. Herrmann, M. Geissler, F. Krausz, and L. Veisz, Phys. Rev. ST Accel. Beams **13**, 091301 (2010).

[6] H. T. Kim, K. H. Pae, H. J. Cha, I. J. Kim, T. J. Yu, J. H. Sung, S. K. Lee, T. M. Jeong, and J. Lee, Phys. Rev. Lett. **111**, 165002 (2013).

[7] W. P. Leemans, A. J. Gonsalves, H.-S. Mao, K. Nakamura, C. Benedetti, C. B. Schroeder, C. Toth, J. Daniels, D. E. Mittelberger, S. S. Bulanov, J. L. Vay, C. G. R. Geddes, and E. Esarey, Phys. Rev. Lett. **113**, 245002 (2014).

[8] J. M. Cole, J. C. Wood, N. C. Lopes, K. Poder, R. L. Abel, S. Alatabi, J. S. J. Bryant, A. Jin, S. Kneip, K. Mecseki, D. R. Symes, S. P. D. Mangles, and Z. Najmudin, Sci. Rep. **5**, 13244 (2015).

[9] E. Guillaume, A. Döpp, C. Thaury, K. Ta Phuoc, A. Lifschitz, G. Grittani, J.-P. Goddet, A. Tafzi, S. W. Chou, L. Veisz, and V. Malka, Phys. Rev. Lett. **115**, 155002 (2015).

[10] O. Lundh, J. Lim, C. Rechatin, L. Ammoura, A. Ben-Ismaïl, X. Davoine, G. Gallot, J.-P. Goddet, E. Lefebvre, V. Malka, and J. Faure, Nat. Phys. **7**, 219 (2011).

[11] A. Buck, M. Nicolai, K. Schmid, C. M. S. Sears, A. Sävert, J. M. Mikhailova, F. Krausz, M. C. Kaluza, and L. Veisz, Nat. Phys. **7**, 543 (2011).

[12] M. Heigoldt, A. Popp, K. Khrennikov, J. Wenz, S. W. Chou, S. Karsch, S. I. Bajlekov, S. M. Hooker, and B. Schmidt, Phys. Rev. ST Accel. Beams **18**, 121302 (2015).

[13] E. Esarey, C. Schroeder, and W. Leemans, Rev. Mod. Phys. **81**, 1229 (2009).

[14] P. Chen, J. M. Dawson, R. W. Huff, and T. Katsouleas, Phys. Rev. Lett. **54**, 693 (1985).

[15] M. J. Hogan, T. O. Raubenheimer, A. Seryi, P. Muggli, T. Katsouleas, C. Huang, W. Lu, W. An, K. A. Marsh, W. B. Mori, C. E. Clayton, and C. Joshi, New J. Phys. **12**, 055030 (2010).

[16] A. Caldwell, K. Lotov, A. Pukhov, and F. Simon, Nat. Phys. **5**, 363 (2009).

[17] C. Bracco, E. Gschwendtner, A. Petrenko, H. Timko, T. Argyropoulos, H. Bartosik, T. Bohl, J. Esteban Müller, B. Goddard, M. Meddahi, A. Pardons, E. Shaposhnikova, F. M. Velotti, H. Vincke, and J. E. Müller, Nucl. Instrum. Methods Phys. Res., Sect. A **740**, 48 (2014).

[18] A. Aschikhin, C. Behrens, S. Bohlen, J. Dale, N. Delbos, L. di Lucchio, E. Elsen, J.-H. Erbe, M. Felber, B. Foster *et al.*, Nucl. Instrum. Methods Phys. Res., Sect. A **806**, 175 (2016).

[19] I. Blumenfeld, C. E. Clayton, F.-J. Decker, M. J. Hogan, C. Huang, R. Ischebeck, R. Iverson, C. Joshi, T. Katsouleas, N. Kirby, W. Lu, K. A. Marsh, W. B. Mori, P. Muggli, E. Oz, R. H. Siemann, D. Walz, and M. Zhou, Nature (London) **445**, 741 (2007).

[20] M. Litos *et al.*, Nature (London) **515**, 92 (2014).

[21] B. Hidding, T. Königstein, J. Osterholz, S. Karsch, O. Willi, and G. Pretzler, Phys. Rev. Lett. **104**, 195002 (2010).

[22] A. Buck, K. Zeil, A. Popp, K. Schmid, A. Jochmann, S. D. Kraft, B. Hidding, T. Kudyakov, C. M. S. Sears, L. Veisz, S. Karsch, J. Pawelke, R. Sauerbrey, T. Cowan, F. Krausz, and U. Schramm, Rev. Sci. Instrum. **81**, 033301 (2010).

[23] C. M. S. Sears, S. B. Cuevas, U. Schramm, K. Schmid, A. Buck, D. Habs, F. Krausz, and L. Veisz, Rev. Sci. Instrum. **81**, 073304 (2010).

[24] F. Dorchies, F. Blasco, T. Caillaud, J. Stevefelt, C. Stenz, A. S. Boldarev, and V. A. Gasilov, Phys. Rev. A **68**, 023201 (2003).

[25] F. Bloch, Ann. Phys. (Berlin) **408**, 285 (1933).

[26] E. Esarey, B. A. Shadwick, P. Catravas, and W. P. Leemans, Phys. Rev. E **65**, 056505 (2002).

[27] M. J. Hogan *et al.*, Phys. Rev. Lett. **95**, 054802 (2005).

[28] N. Barov, J. B. Rosenzweig, M. E. Conde, W. Gai, and J. G. Power, Phys. Rev. ST Accel. Beams **3**, 011301 (2000).

[29] E. Kallos, T. Katsouleas, W. D. Kimura, K. Kusche, P. Muggli, I. Pavlishin, I. Pogorelsky, D. Stolyarov, and V. Yakimenko, Phys. Rev. Lett. **100**, 074802 (2008).

[30] W. Lu, M. Tzoufras, C. Joshi, F. S. Tsung, W. B. Mori, J. Vieira, R. A. Fonseca, and L. O. Silva, Phys. Rev. ST Accel. Beams **10**, 061301 (2007).

[31] A. Martinez de la Ossa, J. Grebenyuk, T. Mehrling, L. Schaper, and J. Osterhoff, Phys. Rev. Lett. **111**, 245003 (2013).

[32] R. Weingartner, M. Fuchs, A. Popp, S. Raith, S. Becker, S. Chou, M. Heigoldt, K. Khrennikov, J. Wenz, T. Seggebrock, B. Zeitler, Z. Major, J. Osterhoff, F. Krausz, S. Karsch, and F. Grüner, Phys. Rev. ST Accel. Beams **14**, 052801 (2011).

[33] R. Weingartner, S. Raith, A. Popp, S. Chou, J. Wenz, K. Khrennikov, M. Heigoldt, A. R. Maier, N. Kajumba, M. Fuchs, B. Zeitler, F. Krausz, S. Karsch, and F. Grüner, Phys. Rev. ST Accel. Beams **15**, 111302 (2012).

[34] R. Fonseca, L. Silva, and F. Tsung, in *Comput. Sci.—ICCS 2002 Lect. Notes Comput. Sci.* (Springer, Berlin, Heidelberg 2002), p. 342.

[35] W. Lu, C. Huang, M. M. Zhou, W. B. Mori, and T. Katsouleas, Phys. Plasmas **12**, 063101 (2005).

[36] L. Gorbunov and V. Kirsanov, Sov. Phys. JETP **18**, 290 (1987).

[37] C. Joshi, B. Blue, C. E. Clayton, E. Dodd, C. Huang, K. A. Marsh, W. B. Mori, S. Wang, M. J. Hogan, C. O'Connell, R. Siemann, D. Watz, P. Muggli, T. Katsouleas, and S. Lee, Phys. Plasmas **9**, 1845 (2002).

[38] H.-C. Wu, T. Tajima, D. Habs, A. W. Chao, and J. Meyer-ter-Vehn, Phys. Rev. ST Accel. Beams **13**, 101303 (2010).

[39] N. Barov and J. B. Rosenzweig, Phys. Rev. E **49**, 4407 (1994).